Polarization selective symmetry breaking in the near-fields of vertical cavity surface emitting lasers

C Degen†, B Krauskopf‡§, G Jennemann†, I Fischer† and W Elsäßer†

† Institute of Applied Physics, Darmstadt University of Technology, Schloßgartenstraße 7, D-64289 Darmstadt, Germany
‡ Department of Engineering Mathematics, University of Bristol, Bristol BS8 1TR, UK
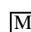
E-mail: B.Krauskopf@bristol.ac.uk

Abstract. We study symmetries in multi-transverse-mode near-fields of circular vertical cavity surface emitting lasers (VCSELs). The $0°$ polarized component of the near-field always has circular or high-order rotational symmetry, indicating that all significant optical properties of the laser are isotropic for light of that polarization. In contrast, the simultaneously present $90°$ polarized part of the same near-field is always symmetrical only upon reflection. This is evidenced by sequences of near-field images of increasing complexity for increasing pump current.

The presence of a preferred direction of the symmetry axis is evidence for a symmetry-breaking anisotropy. We attribute this anisotropy to birefringence, which is induced into any electrically pumped VCSEL by the applied vertical electrical field via the linear electro-optic effect. Thus, the optical index becomes a function of the transverse component of the k-vector of light inside the cavity, which corresponds to an angular dependent index. As the functional dependence on the emission angle is of different strength for orthogonal polarizations, the circular symmetry of the laser is broken only for $90°$ polarized light, while the effect on the $0°$ polarization is too small to affect the near-field.

The highly symmetrical near-field of the unaffected polarization shows remarkable similarities to another physical system of circular symmetry, the static patterns in cellular flames. Our analysis of the symmetry properties of the near-fields has implications for the design of VCSELs as well as for future modelling activities.

Keywords: VCSEL, transverse modes, polarization, birefringence, symmetry-breaking

(Some figures in this article are in colour only in the electronic version; see www.iop.org)

M This article features multimedia enhancements available from the abstract page in the online journal; see www.iop.org.

1. Introduction

Vertical cavity surface emitting lasers (VCSELs) have a number of desirable properties which make them ideal light sources for various technological applications as well as for fundamental physical experiments [1–3]. Their most prominent advantages over edge-emitting diode lasers are longitudinal single-mode emission, low threshold current, high modulation bandwidth and an astigmatism-free circular beam profile. However, there is a trade-off between high output power and the spectral properties of the emitted light: increasing the output power requires increasing laser diameters with the consequence that higher-order transverse modes can be excited and the VCSEL usually emits multiple modes [4–8]. Furthermore, the polarization selectivity in

§ Corresponding author.

circular aperture VCSELs is only weak, which can result in very complex polarization dynamics [9–12]. Both effects are considered negative properties from the applications point of view, where one is often interested in stable high-power emission at the fundamental mode and in a large side-mode suppression ratio. However, these phenomena are also representative for a large variety of effects, which are interesting from the perspective of basic laser physics. An overview of many of these aspects is presented in [13, 14].

In this paper, we study the symmetries of VCSELs' near-fields, which are composed of numerous transverse modes supported by the circular cavity. The high quality of our oxide confined VCSELs enabled us to record near-field images in a wide range of injection currents even well above the thermal roll-over point and all the way to the thermal turn-off, near which we have found modes of

particularly high order. All transverse modes emitted by our VCSELs are linearly polarized along orthogonal axes (in the following referred to as 0° and 90°), a phenomenon which is usually attributed to weak field or strain induced birefringence [15]. Thus, 0° and 90° correspond to the [110] and [1$\bar{1}$0] directions of the (001)-GaAs crystal, respectively, as will be evidenced in section 5. This birefringence also lifts the frequency degeneracy of polarization modes and results in a separation of typically 10–20 GHz. We show that near-field components of orthogonal polarizations have fundamentally different symmetry properties, indicating that the circular symmetry of the VCSEL is selectively broken only for one direction of polarization. Qualitatively, we explain this selective symmetry breaking with electrical field induced birefringence, a mechanism that is well known in semiconductor lasers [16, 17]. However, a connection between birefringence and symmetry breaking in the near-field of VCSELs has not been considered before. According to our hypothesis, polarization selective symmetry breaking is a general feature which we expect to find in any electrically pumped VCSEL. Furthermore, for the near-field of the polarization direction with unperturbed circular symmetry we point out remarkable analogies with the stationary patterns in cellular flames. From these surprising similarities of seemingly unrelated systems we gain further information on the common basic principles of the underlying physics.

The paper is organized as follows. In section 2 we give detailed information on the VCSELs' performance and the experimental setup. Section 3 briefly introduces the notation which is used to classify the symmetry properties of the near-fields in the subsequent parts. Section 4 contains the results of our spectrally and polarization resolved measurements. We classify the symmetries of the near-fields and describe the fundamental differences between orthogonally polarized near-fields. In section 5 we discuss our results and place them in a context with VCSEL-inherent anisotropies. Finally, we compare our lasers with other physical systems of circular symmetry. A summary is given in section 6. The paper also features a multimedia supplement† with colour images and animations of near-fields of increasing complexity.

2. VCSEL structures and experimental setup

The lasers used in our experiments are circular oxide confined GaAs top-emitting VCSELs grown on (001) substrates. They have been fabricated at the University of Ulm and are from the same wafer as the devices described in [18]. The lasers differ only in the diameter of the oxide apertures, with available sizes of 4, 6, 8 and 11 μm, respectively. The VCSELs are operated 'on-wafer', using a needle contact for injecting the pump current, which is supplied by a constant-current source for cw operation. A second needle is used for applying spatially localized pressure to the wafer to investigate the effects of mechanical stress on the VCSELs' performance. The wafer is mounted on a copper plate that is actively stabilized at room temperature. The lasers emit at a wavelength of about 800 nm. In this paper we restrict our discussion to the results obtained from 6 and 11 μm aperture

† Multimedia enhancements are available from the article's abstract page in the online journal; see `www.iop.org`.
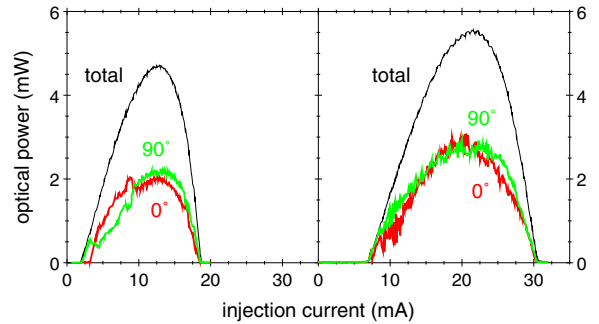
Figure 1. Polarization resolved L/I-graphs of a 6 μm aperture VCSEL (left) and an 11 μm aperture VCSEL (right). The curves represent the integral power and the powers in two orthogonal linear polarizations, as indicated in the figure.
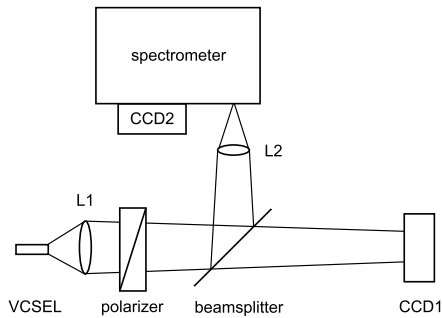
VCSELs. The 4 μm VCSELs turned out to be too small to show high-order modes, and the 8 μm VCSELs behave much like the 6 μm VCSELs.

The polarization resolved light output/current (L/I)-characteristics of the 6 and 11 μm VCSELs are depicted in figure 1. The total optical power of the lasers displays the typical thermal roll-over behaviour. Threshold currents amount to 2 and 6.5 mA, respectively, and the maximum output powers are 4.8 and 5.9 mW. The polarization selection is only weak, so that the total power is almost equally split into the two polarization directions. Similar behaviour has been observed for all lasers on the wafer.

The experimental setup for recording the polarization and spectrally resolved near-field images is shown in figure 2. The near-field of the VCSELs is simultaneously projected onto a CCD camera (CCD1, total near-field images) and onto the input slit of a 1 m Czerny–Turner spectrometer by using a 14.5 mm focal distance collimating objective (Melles–Griot, L1) and a lens of 40 mm focal distance (L2). The exit slit of the spectrometer has been replaced by a second CCD camera (CCD2), which records the spectrally resolved near-field images. Special care has been taken to ensure that the whole spatial extension of the near-field projection passes through the entrance slit without cutting off the edges. Thus, the spectrally resolved images contain both fully two-dimensional spatial information and spectral information along the horizontal axes. The dispersion of the 1200 lines mm^{-1} grating used is sufficient to avoid significant overlap of adjacent transverse modes. Discrimination of orthogonally polarized modes in both the total and the spectrally resolved representation is achieved by insertion of a Glan–Thompson polarizer with an extinction ratio of 10^4. The same polarizer has also been used for the measurement of the L/I-curves. All near-field images have been recorded with exposure times of several microseconds. Thus, possible short-time dynamics are not resolved in our experiment.

3. Symmetry properties of round aperture VCSELs

The VCSELs under investigation have round mesas, metallic contact rings and oxide apertures, i.e. the underlying symmetry of the cavity geometry is circular. Furthermore, in the absence of electrical fields or mechanical strain, GaAs is optically isotropic. This means that, optically and

Figure 2. The experimental setup.

Figure 3. Symmetries of single laser modes. The lines and arrows indicate the axes of rotational and reflectional symmetry.
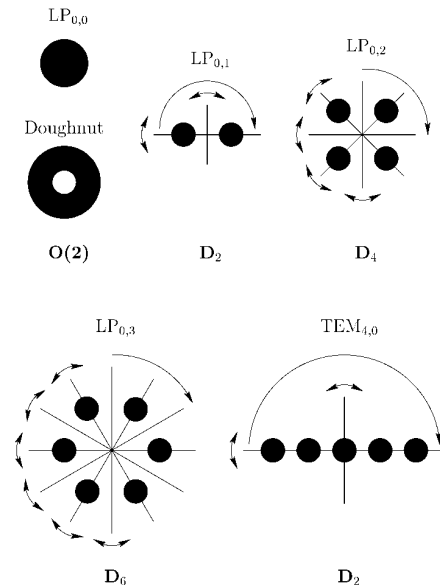
geometrically, the VCSEL (or rather a picture of it from the top) is invariant under rotation by any angle around a vertical axis and by reflection in any straight line through its centre. These operations form the group of rotations and reflections of the Euclidean plane (with respect to the origin), denoted by O(2). The VCSEL having O(2) symmetry means that it is invariant under any element of the group O(2). This symmetry determines the classes of transverse modes possible in the laser. To understand the symmetry properties of the VCSELs' near-fields, we first have to consider the symmetries of the single transverse modes which they are composed of.

Due to the O(2) symmetry, all cavity modes must have the symmetry of a subgroup of O(2). This means that they are Laguerre–Gaussian modes, denoted by $LP_{p,l}$ where p is the radial index and l is the azimuthal index. Geometrically, $2l$ denotes the number of minima in the intensity in the angular direction, and p is the number of minima in the radial direction [19]. If there are no minima in the angular direction then the mode has the full O(2) symmetry of the laser. Examples are the fundamental mode $LP_{0,0}$ and the doughnut mode depicted in figure 3. However, if there are minima in the angular direction ($2l \neq 0$) then the mode does not have full O(2) symmetry. The symmetry group of an $LP_{p,l}$ mode is that of a regular $2l$-gon, denoted by D_{2l}, which is a subgroup of O(2). The group D_{2l} consists of the rotations by integer multiples of π/l and the reflections in $2l$ lines through the origin (the centre of the laser), which means that D_{2l} has $4l$ elements. These symmetries are illustrated in figure 3 for the modes $LP_{0,1}$, $LP_{0,2}$ and $LP_{0,3}$, with symmetry groups D_2, D_4 and D_6, respectively.

If the O(2) symmetry of the cavity is perturbed by an anisotropy, Hermite–Gaussian modes can also be excited†. These modes are denoted by $TEM_{n,m}$ with the parameters n and m counting the numbers of minima in two orthogonal directions. Each of these modes (with $n \neq m$) has as the highest symmetry the group D_2 of a 2-gon. The D_2 symmetry group is also illustrated in figure 3 for a $TEM_{4,0}$ mode.

The VCSELs' near-field is a superposition of several transverse modes, and it is interesting to investigate which modes are excited simultaneously to form the resulting near-field. The overall symmetry of the near-field pattern is the largest common symmetry of the modes involved. In the

case of unperturbed circular symmetry the near-field is a superposition of Laguerre–Gaussian modes. An example is a near-field pattern consisting of a $LP_{0,6}$ and a $LP_{0,2}$ mode, which has overall D_4 symmetry. For perturbed circular symmetry the near-field pattern contains Hermite–Gaussian modes $TEM_{n,m}$ with $n \neq m$, which limits the overall symmetry of the distribution to D_2 symmetry.

4. Experimental results

In this section we present our near-field measurements on 6 μm and 11 μm oxide aperture VCSELs. First, we study the transverse mode structure by resolving the near-fields spectrally. Second, we present polarization resolved images showing how the near-field changes with increasing pump current. The intensities in figures 4–6 are coded in eight-bit grey-scale schemes, which are shown in the respective figures. The brightness represents the relative intensity value so that advantage is taken of the whole dynamical resolution of the CCD camera. The reader is also referred to the multimedia supplement of this work‡, where we present animated depictions that show the evolution of the near-fields with changing injection current. These animations are coded in a eight-bit colour scheme, taking advantage of the additional colour contrast.

4.1. Spectrally resolved near-field images

Spectrally resolved near-field images are depicted in figure 4 for a 6 μm VCSEL at $I = 7.7$ mA (left column) and for an 11 μm VCSEL at $I = 10.5$ mA (right column). The main characteristics are already evident at these currents. At higher pump rates, the mode distributions become very complicated. The first row displays the total near-field, while the images in the second and the third row are of 0° and 90°

---

† In a normal gas or solid state laser, this anisotropy might be induced by only slight misalignments of the mirrors. Thus, Hermite–Gaussian modes are often found in these laser systems, even when they consist of circular apertures, mirrors and active media.

‡ Multimedia enhancements are available from the article's abstract page in the online journal; see www.iop.org.

6µm VCSEL   **11µm VCSEL**

total

0°

90°

λ

$\Delta\lambda = 1$nm
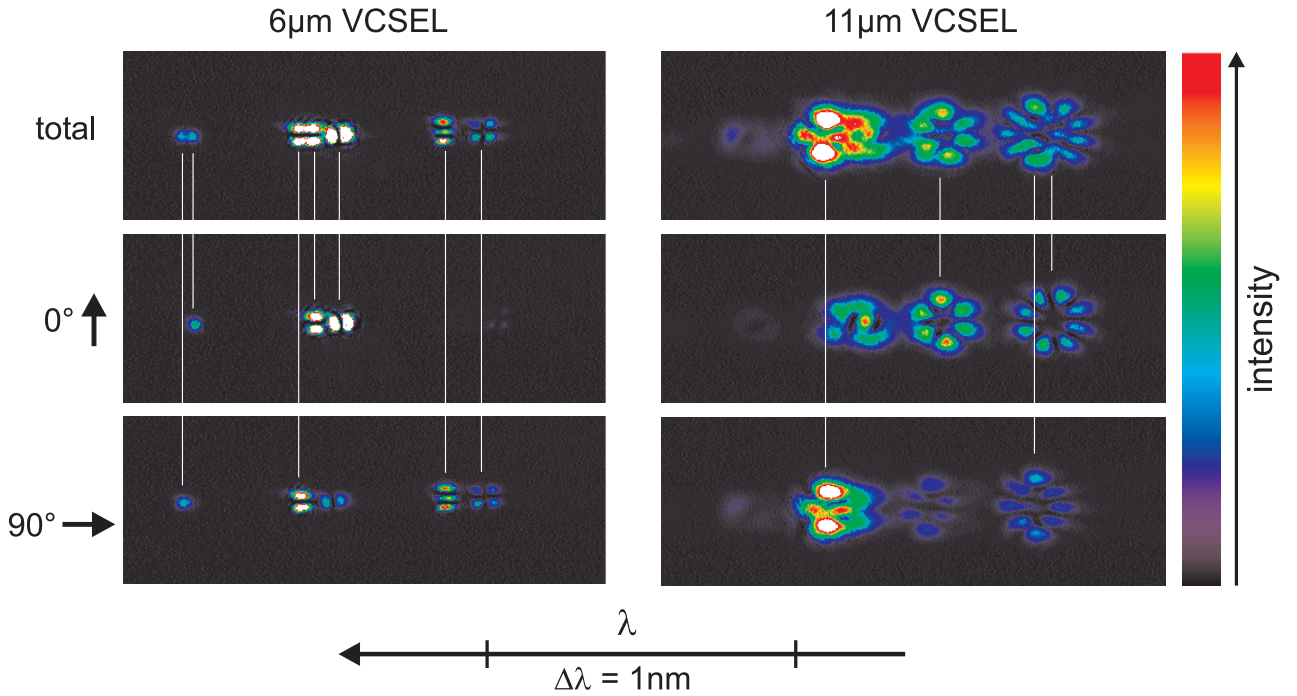
Figure 4. Spectrally resolved near-field images of the 6 μm VCSEL for $I = 7.7$ mA (left) and of the 11 μm VCSEL for $I = 10.5$ mA (right). The first row shows the integral near-field, the second row the 0° polarization and the third row the 90° polarization.

polarization, respectively. The vertical axis represents the spatial coordinate; the horizontal axis is a combination of both spatial and spectral coordinates. As a consequence, spatially extended transverse modes that are only slightly separated in wavelength may overlap in this representation, as can be seen in the top row. The polarization resolved images in the second and the third row on the other hand show practically no overlap of adjacent modes.

The white lines indicate which modes in the total near-field image correspond to the modes in the polarization resolved images. In the 6 μm VCSEL near-fields, a spectral separation of corresponding modes in different polarizations is clearly visible. The spacing between the two TEM$_{0,0}$ modes amounts to $\Delta\lambda = (0.05 \pm 0.01)$ nm. At a central wavelength of $\lambda \approx 800$ nm this corresponds to $\Delta\nu = (23 \pm 4)$ GHz. As the polarization modes are not degenerate, the intensity distributions of both polarizations add up incoherently in the time-avaraged near-fields. Similarly, the non-degenerate modes TEM$_{0,1}$ and TEM$_{1,0}$ in the 0° polarization superimpose incoherently to a doughnut shaped intensity distribution of O(2) symmetry. The resulting doughnut is displayed in figure 5 in the 0° polarization at $I = 4.0$ mA. In contrast, the 90° polarized intensity distribution is governed by a strong TEM$_{0,2}$ mode, which reduces the symmetry of the resulting near-field in this polarization to D$_2$ symmetry along the vertical axis.

The 11 μm VCSEL shown in the right column of figure 4 behaves in a similar way. The single modes that overlap in the total near-field can be discriminated in the images for the two polarization directions. In the 0° near-field the Laguerre–Gaussian modes LP$_{0,3}$ and LP$_{0,4}$ govern the intensity distribution. These modes are of perfectly circular

shape, indicating an O(2) symmetric cavity. In contrast, the near-field in the 90° polarization shows a Hermite–Gaussian mode TEM$_{0,2}$ and Laguerre–Gaussian modes LP$_{0,3}$ and LP$_{0,4}$, which both are clearly of elliptical shape†. The superposition of strong TEM$_{0,m}$ modes and distorted LP modes results in near-fields of D$_2$ symmetry similar to the 6 μm VCSEL. This fundamental difference in the symmetries of the near-field images of 0° and 90° polarization will become even more distinct in the next section, where we concentrate on the symmetries of the orthogonally polarized near-fields at different injection currents.

4.2. Polarization resolved near-field images

We present our near-field measurements in figures 5 and 6. Each row has been recorded for a particular pump current as indicated. The first column contains the linearly polarized part of the near-field in the 0° direction, and the second column that of 90° polarization. As corresponding modes of different polarization are not degenerate in frequency (see section 4.1), the total near-fields (not shown in the figures) are simply superpositions of the intensities in the orthogonal directions of polarization.

In both lasers, the 0° polarized near-fields have O(2) or D$_{2l}$ symmetry with $2l \geqslant 2$, while all 90° polarized near-field images have only D$_2$ symmetry. This observation indicates a selective breaking of the circular symmetry of the laser for light of 90° polarization. We have observed this phenomenon in all VCSELs on the wafer and at almost

---
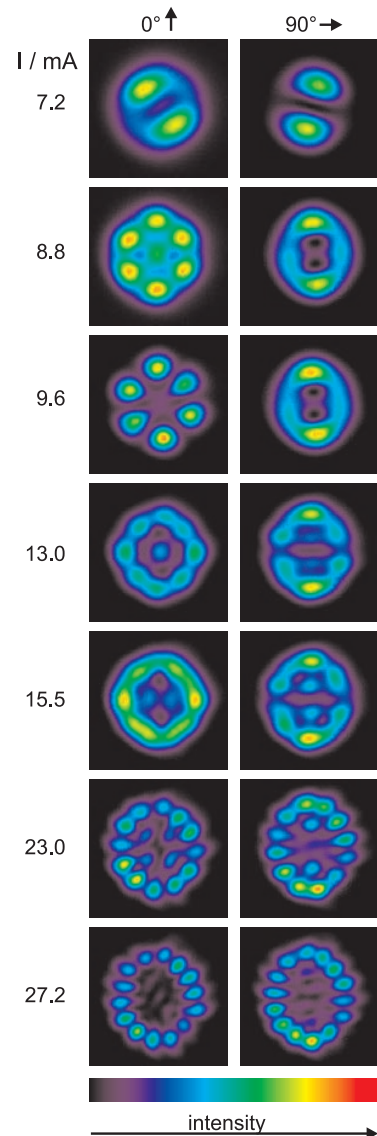
† In the TEM$_{0,2}$ mode the central maximum is almost completely suppressed. This behaviour has been predicted from theoretical modelling by Nakwaski and Sarzala [8].
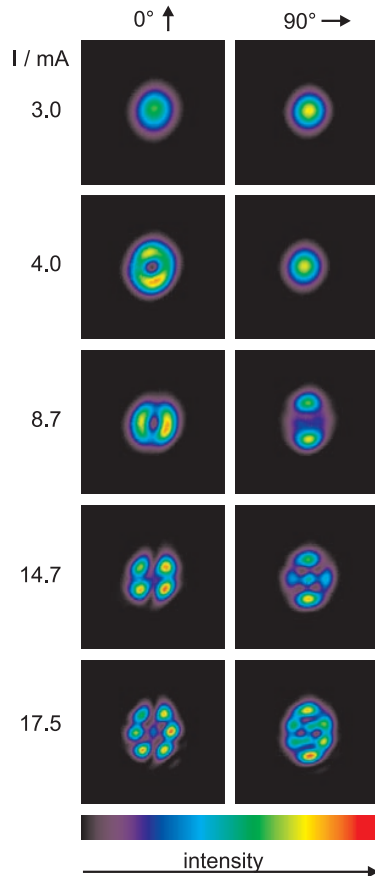
Figure 5. Near-field images of a 6 μm VCSEL at pump currents as indicated. The first column shows the 0° polarized near-field and the second column the 90° polarized near-field.

Figure 6. Near-field images of an 11 μm VCSEL at pump currents as indicated. The first column shows the 0° polarized near-field and the second column the 90° polarized near-field.

any injection current. The only exceptions have been found at very low injection currents, where the intensity distributions in both polarizations are determined by the same low-order transverse mode and at very high injection currents near the thermal turn-off. There, both near-fields contain only one high-order Laguerre–Gaussian mode, which is distorted to an elliptical shape, where the strength of distortion depends on the polarization. At any intermediate injection current the fundamental difference in symmetry is clearly visible. It is remarkable that we have found this polarization selective symmetry breaking to affect not the polarization ratio (compare with figure 1) but only the near-field symmetries. We will propose an explanation for the symmetry breaking in section 5.

Details of the transverse modes that determine the near-field images at the respective injection currents are given in table 1. In addition, the symmetries of the resulting near-fields are also indicated. It may be suprising at first sight that the modes in the 90° polarization for the 6 μm VCSEL for 8.7 mA, and for the 11 μm VCSEL for 8.8, 9.6 and 23.0 mA are indicated as $TEM_{0,2}$. However, in these modes again the central maximum is suppressed, as has been predicted theoretically and observed experimentally for Hermite–Gaussian modes of even order [8,20]. Furthermore, it is non-trivial that at very high injection currents only single Laguerre–Gaussian modes of high order determine the near-fields (usually called 'daisy modes' [21]). The

reason for this behaviour is the complex interaction of current spreading, current crowding near the oxide perimeter, spatial and spectral hole burning and the influence of thermal gradients in the laser [8, 20, 22–25]. The net result is an increase of gain in a ring shaped area at the borders of the laser and a suppression of the gain in the centre, which leads to a preference for high-order Laguerre–Gaussian modes.

5. Discussion

The results of section 4 show very conclusively fundamentally different symmetry properties of the two orthogonally polarized near-fields, corresponding to a polarization selective symmetry breaking that must be caused by some kind of anisotropy. We have performed further experiments to identify the source of the anisotropy. First, we have applied mechanical pressure to the VCSEL by positioning a second needle on the wafer at different coordinates close to the laser.

Table 1. Transverse modes in the near-fields and resulting near-field symmetries at the indicated injection currents.

I (mA)	0° polarization	90° polarization
	6 μm VCSEL	
3.0	$TEM_{0,0} \rightarrow O(2)$	$TEM_{0,0} \rightarrow O(2)$
4.0	$TEM_{1,0}TEM_{0,1} \rightarrow O(2)$	$TEM_{0,0} \rightarrow O(2)$
8.7	$TEM_{1,0}TEM_{1,1} \rightarrow D_2/D_4$	$TEM_{0,2} \rightarrow D_2$
14.7	$TEM_{1,1} \rightarrow D_4$	$TEM_{1,0}TEM_{0,2} \rightarrow D_2$
17.5	$TEM_{0,0}TEM_{1,2} \rightarrow D_2$	$TEM_{2,1}TEM_{0,3} \rightarrow D_2$
	11 μm VCSEL	
7.2	$TEM_{0,1} \rightarrow D_2$	$TEM_{0,1} \rightarrow D_2$
8.8	$TEM_{0,0}LP_{0,3} \rightarrow D_6$	$TEM_{1,0}TEM_{0,2} \rightarrow D_2$
9.6	$LP_{0,3} \rightarrow D_6$	$TEM_{1,0}TEM_{0,2} \rightarrow D_2$
13.0	$TEM_{0,0}LP_{0,4} \rightarrow D_8$	$TEM_{2,1}TEM_{0,3} \rightarrow D_2$
15.5	$TEM_{3,0}LP_{0,3} \rightarrow D_2$	$TEM_{2,1}TEM_{0,3} \rightarrow D_2$
23.0	$TEM_{1,1}LP_{0,6} \rightarrow D_4$	$TEM_{0,2}LP_{0,6} \rightarrow D_2$
27.2	$LP_{0,7} \rightarrow D_2^a/D_{14}$	$TEM_{0,3}LP_{0,7} \rightarrow D_2$

[a] The symmetry of a 'pure' $LP_{0,7}$ mode is D_{14}; at the very highest injection current, however, even the 0° polarized near-field shows a slight distortion into an ellipse-like shape as a consequence of the strong vertical pump field. Thus, the symmetry of this near-field might already be considered as reduced to D_2.

However, the polarization ratio, the orientation of the transverse modes and the injection currents at which the individual modes appear have been entirely unaffected. Hence, we can exclude mechanical stress from the contact needle as a source of the anisotropy. Furthermore, we have carefully checked the experimental setup to make sure that optical feedback to the VCSEL from optical surfaces in the beam does not have significant influence.

Instead, we propose to consider field induced birefringence as the source of the anisotropy. Birefringence is induced into the laser by the static vertical electrical field via the linear electro-optic effect. A possible impact of this anisotropy on the polarization ratio has already been investigated in the past [16, 17]. However, we relate the field induced birefringence to the symmetries in near-field distributions, which is a new aspect. The aim of this discussion is to corroborate the general validity of our hypothesis by comparing the strength of the underlying effects. A detailed numerical analysis of the microscopic VCSEL properties and their impact on the near-field symmetries will be a demanding task for future work.

In any VCSEL a static vertical electrical field is always present due to the vertically injected current. The strength of this field depends on the resistance of the VCSEL and can amount typically to 10^7 V m^{-1} across the whole structure. Without this field the index of refraction is isotropic and the indicatrix (see, for example, [26]) is given by

$$\frac{n_x^2 + n_y^2 + n_z^2}{n_0^2} = 1, \quad (1)$$

where x, y and z are the crystal axes with z aligned along the vertical [001] direction, and n_0 is the optical index without a static electrical field. In this representation, the optical index n for light with an electric field vector $\vec{\mathcal{E}}$ is given by $n = |\vec{n}| = \sqrt{n_x^2 + n_y^2 + n_z^2}$, with $\vec{n} \| \vec{\mathcal{E}}$ pointing at the surface of the indicatrix.

The presence of the static vertical electrical field E_z modifies the indicatrix to

$$\frac{n_x^2 + n_y^2 + n_z^2}{n_0^2} + 2r_{41}E_z n_x n_y = 1, \quad (2)$$

where $r_{41} \approx 10^{-12}$ m V^{-1} is a component of the electro-optic tensor for GaAs [27]. A rotation of the coordinate system by 45° about the z-axis changes to the symmetry axes of the ellipsoid: $x' = [1\bar{1}0]$ and $y' = [110]$. In this coordinate system equation (2) becomes

$$\left(\frac{1}{n_0^2} - r_{41}E_z\right)n_{x'}^2 + \left(\frac{1}{n_0^2} + r_{41}E_z\right)n_{y'}^2 + \left(\frac{1}{n_0^2}\right)n_z^2 = 1. \quad (3)$$

Using $r_{41}E_z \ll 1/n_0^2$ as an approximation, one obtains

$$n(\vec{\mathcal{E}} = \mathcal{E}_{x'}) \approx n_0 + \frac{n_0^3}{2}r_{41}E_z,$$
$$n(\vec{\mathcal{E}} = \mathcal{E}_{y'}) \approx n_0 - \frac{n_0^3}{2}r_{41}E_z, \quad (4)$$
$$n(\vec{\mathcal{E}} = \mathcal{E}_z) = n_0.$$

So, the index in the [1$\bar{1}$0] direction becomes maximal while the index in the [110] direction is smallest.

From equation (4), we obtain $\Delta n = n(\vec{\mathcal{E}} = \mathcal{E}_{x'}) - n(\vec{\mathcal{E}} = \mathcal{E}_{y'}) \approx 4 \times 10^{-4}$ as the value of the birefringence induced by the electro-optic effect. On the other hand, we can calculate the birefringence Δn from the wavelength difference $\Delta\lambda$ between the fundamental transverse modes in the two orthogonal polarizations, by using

$$\frac{\Delta\lambda}{\lambda} = \Gamma\frac{\Delta n}{n_0}, \quad (5)$$

where Γ is the confinement factor [28]. Assuming a confinement factor of $\Gamma = 0.5$, and using the experimental data, $\Delta\lambda = 0.05$ nm, $\lambda = 800$ nm and $n_0 = 3.5$, also results in $\Delta n \approx 4 \times 10^{-4}$. These values are obtained by rough estimation, as the uncertainties of both Γ and E_z are in the range of at least 50%. So, both values of Δn also have a minimum uncertainty of 50%. However, both experimentally and theoretically obtained values are of the same order of magnitude, which confirms our hypothesis that the observed birefringence indeed can be induced in the VCSEL by the applied electrical field in agreement with [17].

A further consequence of equation (5) is that a change in index causes a change in wavelength of the same sign. A comparison with figure 4 yields that modes of 90° polarization are of higher wavelength than corresponding modes of 0° polarization. So we conclude that the 90° direction (higher wavelength—larger index) corresponds to the [1$\bar{1}$0] direction, and the 0° direction (lower wavelength—smaller index) corresponds to the [110] direction. With this classification, we can also qualitatively explain the different symmetry properties of intensity distributions in orthogonal polarizations using equations (3) and (4). Let us first consider 90° polarized light, i.e. light with a k-vector parallel to the [001]-axis and an $\mathcal{E}$-vector parallel to the [1$\bar{1}$0]-axis. The index for this light is $n(\vec{\mathcal{E}} = \mathcal{E}_{x'}) = n_0 + \frac{n_0^3}{2}r_{41}E_z$. If the laser

emits in a higher-order transverse mode, then the k-vector deviates slightly from the [001] direction, i.e. it also has a transverse component. For a transverse component of the k-vector in the [110] direction (i.e. the 0° direction) the $\mathcal{E}$-vector still points in the [1$\bar{1}$0] direction and so the optical index remains constant. On the other hand, a transverse component of the k-vector in the [1$\bar{1}$0] direction is equivalent to a deviation of the $\mathcal{E}$-vector from the [1$\bar{1}$0] direction, so that the index becomes smaller. In other words, for light of 90° polarization the index n remains constant for a k-vector with a component in the [110] direction (i.e. the 0° direction) but decreases for a k-vector with a component in the [1$\bar{1}$0] direction (i.e. the 90° direction). This angular-dependent optical index is equivalent to a mirror that is flat in the 0° direction and concave in the 90° direction, only for 90° polarized light. The plane–concave mirror causes a concentration of the 90° polarized intensity in the 90° direction as is evident from figures 5 and 6. The same mechanism also affects light of 0° polarization, where a transverse component of the k-vector in the 0°-direction [110] causes an increase of the index, which again is equivalent to a plane–convex mirror for 0° polarized light. From the experimental data, however, it is clearly evident that the effect on the 90° polarized near-field is by far stronger than that on the 0° near-field, the latter being slightly distorted into an ellipse-like shape only at the highest injection current. This agrees with the angular dependence of the optical index that is of different strength for orthogonal polarizations. In order to estimate this difference, we now consider projections of the indicatrix (equation (3)) onto the planes $n_x = 0$ and $n_y = 0$. Then, we transform the projections to circular coordinates of the respective planes, n and ϕ, and investigate how $n|_{n_x=0}$ and $n|_{n_y=0}$ change with the angle ϕ. For the sake of simplicity we only calculate the derivatives $\frac{dn^2}{d\phi}|_{n_x=0}$ and $\frac{dn^2}{d\phi}|_{n_y=0}$ of n^2. Using the transformation $n_z = n \sin\phi$ and $n_x|_{n_y=0} = n\cos\phi$, $n_y|_{n_x=0} = n\cos\phi$, we obtain

$$\left.\frac{dn^2}{d\phi}\right|_{n_x=0} = \frac{2r_{41}E_z \sin\phi\cos\phi}{(C_+\cos^2\phi + 1/n_0^2 \sin^2\phi)^2}, \qquad (6)$$

$$\left.\frac{dn^2}{d\phi}\right|_{n_y=0} = -\frac{2r_{41}E_z \sin\phi\cos\phi}{(C_-\cos^2\phi + 1/n_0^2 \sin^2\phi)^2} \qquad (7)$$

$$C_{\pm} = \frac{1}{n_0^2} \pm r_{41}E_z. \qquad (8)$$

As $C_+ \geqslant C_-$, we find

$$\left|\left.\frac{dn^2}{d\phi}\right|_{n_y=0}\right| \geqslant \left|\left.\frac{dn^2}{d\phi}\right|_{n_x=0}\right|. \qquad (9)$$

Physically, this means that for transverse modes of 90° polarization the effective curvature of the mirrors (i.e. the anisotropy) is larger than that for 0° polarized light. In the case of our VCSELs, only the curvature for 90° polarization is large enough to break the laser's circular symmetry, while for 0° polarization the effect is too small to modify the near-fields in a measurable way. The positive sign of equation (6) indicates a convex mirror curvature for 0° polarized light, while the negative sign of equation (7) indicates a concave mirror for the 90° polarization, which also agrees with

the experimental data. Admittedly, the relative difference between C_+ and C_- amounts to only 10^{-4} and thus appears very small at first sight. However, it has been demonstrated, in numerous experiments, that VCSEL performance is very sensitive to even extremely small anisotropies. For example, polarization orientation or polarization suppression has been modified by anisotropies one to three orders of magnitude smaller than in our lasers [29, 30]. Thus, it seems reasonable to consider field induced birefringence as the source of the polarization selective symmetry breaking.

According to our hypothesis, the polarization selective anisotropy is inherent in the VCSEL structure and therefore has to be expected to modify the near-field symmetries of any transverse multi-mode VCSEL on a (001) substrate. Besides the fundamental physical significance, this effect also has technological consequences. Different attempts have been made to stabilize a VCSEL on a single linear polarization [31, 32]. Our conclusions indicate that for any application that requires circular near-fields rather than elliptical ones, for example fibre coupling, the [110] polarization should be chosen as the lasing polarization and the [1$\bar{1}$0] polarization should be suppressed.
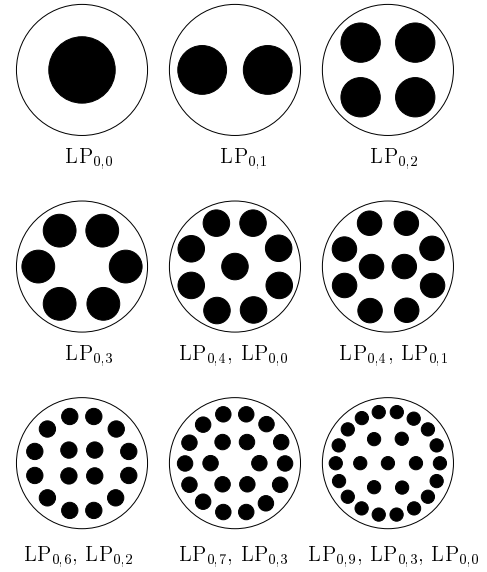
The results of section 4 show very conclusively a fundamental difference in the symmetry properties of the two orthogonal polarized near-fields. It is particularly striking that the VCSEL's geometrical O(2) symmetry is selectively broken and reduced to a D_2 symmetry for light of 90° polarization, while the full O(2) symmetry of the system simultaneously remains unaffected for 0° polarized light, at least at low to intermediate injection currents. Further strong support for this conclusion comes from the fact that similar sequences of patterns as in our VCSELs have been found in seemingly unrelated systems with circular symmetry. Many systems with O(2) symmetry have been studied, for example the Taylor–Couette experiment (see [33, 34] and further references therein) and the circular hydraulic jump [35, 36]. In the study of transverse modes in a CO_2 laser some subgroups of O(2) have been identified as symmetries [37, 38], but the example closest to the VCSEL patterns considered here is the stationary patterns in cellular flames in a circular burner observed by Gorman *et al* [39]. One image with typical patterns from their experiments is reproduced in figure 7. In this image, one can see regions of high temperature in the gas flames (regions of high brightness in the images) competing for the common reservoir of oxygen. As a consequence, this characteristic sequence of highly symmetric patterns with increasing complexity is found when increasing the gas flow rate. Competition for a common reservoir is a common principle in physics, and it is also crucial for the formation of the near-field distribution in a laser. In fact, the near-field observed is the combination of transverse modes that uses the common gain reservoir in the laser in the most efficient way. For increasing pump current this leads to near-field patterns of increasingly complex symmetry. In figure 8 we present a schematical complete sequence of near-field patterns that have all been observed in our 11 μm VCSELs (most of them can be found in figure 6). This sequence exhibits a striking structural similarity to the sequence in figure 7. However, there is an important difference between the near-field of a VCSEL
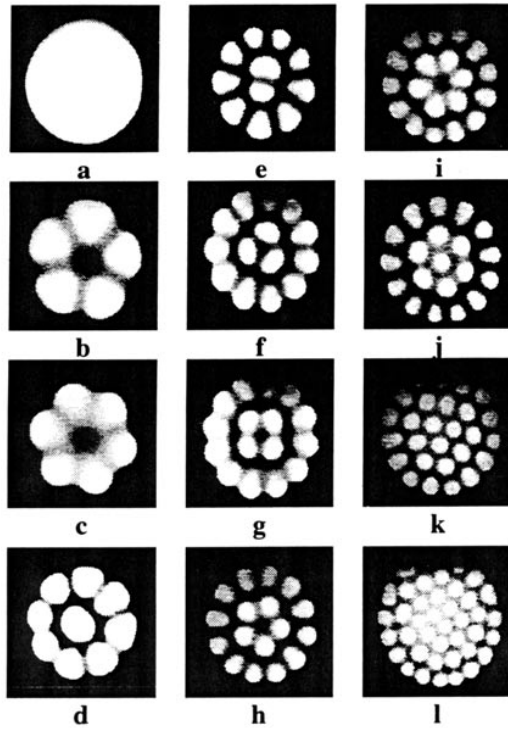
Figure 7. Ordered states in cellular flames as observed by Gorman *et al* (reproduced from [39] with kind permission by Gordon and Breach Publishers, copyright held by OPA (Overseas Publishers Association) NV). The figure shows different stationary patterns arising from a gas flame beneath a glass plate. With the gas flow rate as the parameter under variation one observes highly symmetric patterns of increasing complexity.

Figure 8. Schematical depiction of a sequence of near-field patterns composed of different Laguerre–Gaussian modes for a VCSEL in the $0°$ polarization with perfect O(2) symmetry for increasing pump current I.

and the flame patterns. In the flame experiment the only restriction in the competition for the common resource is the O(2) symmetry of the burner. On the other hand, near-fields of VCSELs are superpositions of *laser modes*, which is an additional restriction. The $0°$ near-fields consist of Laguerre–Gaussian $LP_{0,n}$ modes, which always have an even number of maxima. In other words, the sequence in figure 8 is a subsequence of the respective sequence of flame patterns, of which 12 are depicted in figure 7. This becomes evident by comparing figure 7 with the second column of figure 6, which shows that (c) agrees with $I = 9.6$, (d) with $I = 13.0$, (e) with $I = 15.5$ and (g) with $I = 23.0$ mA. On the other hand, for example, the patterns of figures 7(b), (f) and (h) cannot occur as near-fields because they are not composed of laser modes.

Apart from this restriction, the comparison with the flame experiment shows that the near-field patterns in the $0°$ polarization are a classical example of competition in an O(2) symmetric system. This is quite astonishing since simultaneously and in the same laser the symmetry for light of $90°$ polarization is selectively broken. These observations have significant implications for future modelling of VCSELs. We conclude that for modelling spatial intensity distributions, the VCSEL initially should be considered as an O(2) symmetric system consisting of two O(2) symmetric subsystems for the orthogonal directions of linear polarization, which are coupled via the gain reservoir as proposed by the spin-flip model [9]. The selective symmetry

breaking for light of $90°$ polarization then enters the system as optical anisotropy of the cavity via an angular dependent optical index, while the O(2) symmetry of the $0°$ subsystem remains unaffected. Since the symmetry breaking is localized in the $90°$ polarization we propose to call this phenomenon *localized symmetry breaking*. It remains a challenge for future work to develop a consistent model for VCSELs that is able to reproduce the observed near-field patterns presented in this work.

6. Summary

We have presented spectrally and polarization resolved measurements of near-fields of circular aperture oxide confined VCSELs of 6 and 11 μm diameter. Our experiments show clearly that for $0°$ polarized light the VCSEL is a system of unperturbed circular symmetry O(2) while for $90°$ polarized light the symmetry is broken and reduced to D_2. This polarization dependent symmetry breaking can be explained by birefringence that is induced into the VCSEL by the vertical electrical field via the linear electro-optic effect. The electrical field changes the shape of the indicatrix to an ellipsoid. Thus, transverse components in the k-vector of light inside the cavity lead to changes in the optical index. The effect is of different strength for light polarized in the [110] and the [1$\bar{1}$0] directions because of different curvatures of the indicatrix in the respective directions. This leads to a polarization dependent anisotropy. For light of $0°$ polarization the O(2) symmetry seems to be affected so weakly that deviations from the O(2) symmetry cannot be observed experimentally. As a consequence, the sequence of intensity distributions in the near-field is of remarkable similarity to stationary patterns in cellular flames, which is a quite different example of a system with O(2) symmetry. From our experiments, we obtain basic information on the physics of semiconductor VCSELs with consequences

for future laser design. We also conclude that symmetry considerations, and in particular the localized symmetry breaking in the 90° polarization, need to be included in future models of VCSELs.

Acknowledgments

References

[1] Ebeling K-J, Fiedler U, Michalzik R, Reiner G and Weigl B 1996 *Int. J. Electron. Commun.* **50** 316
[2] Giboney K S, Aronson L B and Lemoff B E 1998 *IEEE Spectrum* **2** 43
[3] Degen C, Vey J-L, Elsäßer W, Schnitzer P and Ebeling K-J 1998 *Electron. Lett.* **34** 1585
[4] Epler J E, Gehrsitz S, Gulden K H, Moser M, Sigg H C and Lehmann H W 1996 *Appl. Phys. Lett.* **69** 722
[5] Li H, Lucas T L, McInerney J G and Morgan R A 1994 *Chaos Solitons Fractals* **4** 1619
[6] Chang-Hasnain C J, Harbison J P, Hasnain G, Von Lehmen A C, Florez L T and Stoffel N G 1991 *IEEE J. Quantum Electron.* **27** 1402
[7] Hörsch I, Kusche R, Marti O, Weigl B and Ebeling K-J 1996 *J. Appl. Phys.* **79** 3831
[8] Nakwaski W and Sarzala R P 1998 *Opt. Commun.* **148** 63
[9] San Miguel M, Feng Q and Moloney J V 1995 *Phys. Rev.* A **52** 1728
[10] Hofmann H F and Hess O 1997 *Phys. Rev.* A **56** 868
[11] Martin-Regalado J, San Miguel M and Abraham N B 1996 *Opt. Lett.* **21** 351
[12] van Exter M P, Willemsen M B and Woerdman J P 1998 *Phys. Rev.* A **58** 4191
[13] Lugiato L A and El Naschi M S (ed) 1994 Nonlinear optical structures, patterns, chaos *Chaos Solitons Fractals* **4** (8/9 special issue)
[14] Weiss C O, Vaupel M, Staliunas K, Slekys G and Taranenko V B 1999 *Appl. Phys.* B **68** 151
[15] Woerdman J P, Jansen van Doorn A K and van Exter M P 1997 *Laser Phys.* **7** 63
[16] van Exter M P, Jansen van Doorn A K and Woerdman J P 1997 *Phys. Rev.* A **56** 845
[17] Hendriks R F M, van Exter M P, Woerdman J P, van Geelen A, Weegels L, Gulden K H and Moser M 1997 *Appl. Phys. Lett.* **71** 2599
[18] Jung C, Jäger R, Grabherr M, Schnitzer P, Michalzik R, Weigl B, Müller S and Ebeling K J 1997 *Electron. Lett.* **33** 1790
[19] Siegman A E 1986 *Lasers* (Mill Valley, CA: University Science)
[20] Degen C, Fischer I and Elsäßer W 1999 *Opt. Express* **5** 38
[21] Pereira S F, Willemsen M B, van Exter M P and Woerdman J P 1998 *Appl. Phys. Lett.* **73** 2239
[22] Zhao Y G and McInerney J G 1996 *IEEE J. Quantum Electron.* **32** 1950
[23] Vakhshoori D, Wynn J D, Zydzik G J, Leibenguth R E, Ascom M T, Kojima K and Morgan R A 1993 *Appl. Phys. Lett.* **62** 1448
[24] Wilson G C, Kuchta D M, Walker J D and Smith J S 1994 *Appl. Phys. Lett.* **64** 542
[25] Degen C, Fischer I and Elsäßer W 2000 *Appl. Phys. Lett.* **76** 3352
[26] Lipson S G, Lipson H and Tannhauser D S 1995 *Optical Physics* (Cambridge: Cambridge University Press)
[27] Yariv A and Yeh P 1984 *Optical Waves in Crystals* (New York: Wiley)
[28] Vakhshoori D and Leibenguth R E 1995 *Appl. Phys. Lett.* **67** 1045
[29] Jansen van Doorn A K, van Exter M P and Woerdman J P 1996 *Appl. Phys. Lett.* **69** 1041
[30] Park M S, Ahn B T, Yoo B-S, Chu H Y, Park H-H and Chang-Hasnain C J 2000 *Appl. Phys. Lett.* **76** 813
[31] Jansen van Doorn A K, van Exter M P and Woerdman J P 1996 *Appl. Phys. Lett.* **69** 3635
[32] Ha K-H, Lee Y H, Shin H-K, Lee K-H and Whang S-M 1998 *Electron. Lett.* **34** 1401
[33] Golubitsky M and Schaeffer D G 1985 *Singularities and Groups in Bifurcation Theory* vol 1 (New York: Springer)
[34] Golubitsky M, Stuart I and Schaeffer D G 1988 *Singularities and Groups in Bifurcation Theory* vol 2 (New York: Springer)
[35] Ellegaard C, Hansen A E, Haaning A, Hansen K, Marcussen A, Bohr T, Hansen J L and Watanabe S 1998 *Nature* **392** 767
[36] Ellegaard C, Hansen A E, Haaning A, Hansen K, Marcussen A, Bohr T, Hansen J L and Watanabe S 1999 *Nonlinearity* **12** 1
[37] Green C, Mindlin G B, D'Angelo E J, Solari H G and Tredicce J R 1990 *Phys. Rev. Lett.* **65** 3124
[38] D'Angelo E J, Izaguirre E, Mindlin G B, Huyet G, Gil L and Tredicce J R 1992 *Phys. Rev. Lett.* **68** 3702
[39] Gorman M, El-Hamdi M and Robbins K A 1994 *Combust. Sci. Technol.* **99** 37